Sensors and Actuators A 254 (2017) 78–88

Contents lists available at ScienceDirect

Sensors and Actuators A: Physical

journal homepage: www.elsevier.com/locate/sna

Efficiency of end effect probes for *in-situ* permittivity measurements in the 0.5–6 GHz frequency range and their application for organic soil horizons study

François Demontoux[a,*], Stephen Razafindratsima[f], Simone Bircher[b], Gilles Ruffié[a], Fabrice Bonnaudin[a], François Jonard[c,d], Jean-Pierre Wigneron[e], Mehdi Sbartaï[f], Yann Kerr[b]

[a] *IMS Laboratory, University of Bordeaux, 16 Avenue Pey Berland 33607 Pessac, France*
[b] *Centre d'Etudes Spatiales de la Biosphère, Toulouse, France*
[c] *Agrosphere (IBG-3), Institute of Bio- and Geosciences Forschungszentrum Jülich GmbH, Jülich, Germany*
[d] *Earth and Life Institute, Université catholique de Louvain, Louvain-la-Neuve, Belgium*
[e] *INRA, UMR 1391 ISPA, F-33140 Villenave d'Ornon, France*
[f] *I2M Laboratory, GCE Department, University of Bordeaux, Bordeaux, France*

ARTICLE INFO

Article history:
Received 12 July 2016
Received in revised form 1 November 2016
Accepted 6 December 2016
Available online 9 December 2016

Keywords:
Permittivity
End effect probe
Organic soil
Moisture
Remote sensing

ABSTRACT

The remote signatures measured at microwave frequency above land surfaces are strongly dependent on the permittivity of the soil, which is linked to its moisture content. Thus, soil permittivity is a key parameter when algorithms are developed for the retrieval of hydrologic parameters from remote sensing data. Soil permittivity measurements are generally carried out in the laboratory because *in-situ* measurements are more difficult to obtain. The study presents the development of two probes (N and SMA probes) for *in situ* soil permittivity measurements (*i.e.* measurements of dielectric properties). They are based on the end effect phenomenon of a coaxial waveguide and so are called end effect probes in this paper. Results obtained on well-known materials (water and polytetrafluoroethene) are compared with corresponding data obtained by laboratory approaches (Von Hippel's method and resonant cavity) and show good agreement from 0.5 GHz up to ~3.5 GHz and 6 GHz for N and SMA probes respectively. Then measurements made on concrete and mineral soil are reported to underline the efficiency of end effect probes for *in-situ* dielectric measurements. Finally, through work undertaken in the framework of the European Space Agency's SMOSHiLat project, we demonstrate the applicability of the two probes for measurements performed within these frequency ranges in complex material such as organic soil horizons.

1. Introduction

Microwave remote sensing has proved to be a powerful tool to provide soil moisture information on a large scale. The remote electromagnetic (EM) signatures measured at microwave frequencies above land surfaces are strongly dependent on the soil permittivity, especially at L-Band. To retrieve soil moisture, advantage is taken of the large difference between the relative permittivity (referred to as permittivity in the following) of the dry soil and water. Furthermore, soil permittivity also depends on parameters such as texture, temperature, frequency measurement and soil bulk density. The use of experimental setups such as a resonant cavity [1,2] or waveguide systems ([3,4]) allows measurements to be made in the laboratory for various conditions (such as temperature and moisture), types of soil and ranges of frequencies. Dielectric mixing models such as the ones developed by Dobson et al. [5,6] or Mironov et al. [7–10] enable mineral soil permittivity to be estimated but these models are limited to a low frequency range and do not necessarily give acceptable results outside the validity area in terms of soil types. In particular, they have to be adjusted for organic soils, because these media haven't been take precisely into consideration yet.

Some *in situ* measurement probes based on permittivity properties of soil exist (*e.g.* Time Domain Reflectometers (TDR) and Transmissometers (TDT), capacitance and impedance sensors) [11–14]. They are dedicated to the acquisition of soil moisture data

* Corresponding author.
E-mail address: francois.demontoux@u-bordeaux.fr (F. Demontoux).

http://dx.doi.org/10.1016/j.sna.2016.12.005
0924-4247/

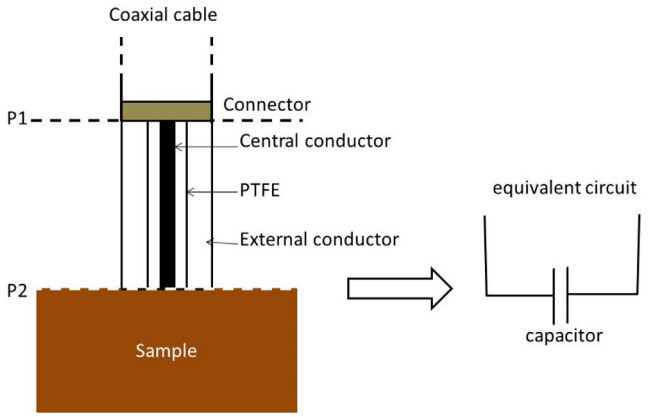

Fig. 1. Overview of the end effect probe measurement system.

based on permittivity estimations over a range of frequencies from around 50 MHz to 1 or 2 GHz. Other Dielectric Assessment Kits exist but they are expensive and they are rather dedicated to laboratory measurement. Furthermore, the user can't modify the probe or the data processing program to address specific issues related to particular materials (organic soils) or specific measurement conditions (*in situ* long time records).

The present study describes an *in situ* dielectric measurement system using probes based on the end effect phenomenon of an open coaxial waveguide and so are called end effect probes in this paper. The probes are presented and dielectric measurements obtained for well-known materials (water, polytetrafluoroethene PTFE) are discussed. Measurements were also made on concrete and mineral soil (silt loam) samples because they are respectively easy to produce and easy to collect and preserve in the laboratory. In both cases, samples used for the measurements presented have been prepared to be very similar to the *in-situ* material in term of bulk density or heterogeneity. Then the efficiency of end effect probes for *in-situ* dielectric measurements is discussed. Finally, the potential use of this technique for *in situ* permittivity measurement of complex media such as organic soil layers is evaluated within the scope of the SMOSHiLat project (European Space Agency's Changing Earth Science Network) [15]. SMOSHilat is closely linked to the Soil Moisture and Ocean Salinity (SMOS) space mission [16–18], the objective of which is the retrieval of soil moisture information using L-band microwave (1.4 GHz) brightness temperature (TB) observations. The retrieval is based on the inversion of the L-band Microwave Emission of the Biosphere (L-MEB) model using parameters defined from studies in dry and temperate climate conditions. Therefore, the SMOSHiLat project was carried out to improve our understanding of L-band emissions and support SMOS data quality in northern climate zones covered by pronounced organic surface layers. One of the project goals is to establish a database including L-band dielectric constant measurements of organic-rich soils from different northern sites (Finland, Denmark, Scotland, Russia) and thus enable the dielectric estimation models (*e.g.* Dobson and Mironov) to be extended to consider organic soil types.

The results are discussed and the potential interest of the *in situ* measurement technique is evaluated.

2. Material and method

2.1. End effect probe method

An end effect probe consists of a coaxial cable in contact with a sample (Fig. 1). The system (*i.e.* coaxial end and material in contact) can be modeled as a capacitor ([19] Stuchly and Stuchly).

The value of this capacitor can be defined by:

$$C = C_0 \varepsilon^b \tag{1}$$

where C is the equivalent capacitor, C_0 and b are the probe parameters and are defined on the basis of measurements on well-known materials, ε is the relative complex permittivity of the sample. In this paper we will express it as:

$$\varepsilon = \varepsilon' + j.\varepsilon'' \tag{2}$$

The complex admittance of the circuit is Y and is expressed as:

$$Y = j\omega C_0 \varepsilon^b \tag{3}$$

with $\omega = 2\pi f$

The reflection coefficient S_{11e} at the surface of the probe in air (without contact with a material) is defined by:

$$S_{11e} = \frac{Y_0 - Y}{Y_0 + Y} = \frac{1 - jC_0Z_0\omega}{1 + jC_0Z_0\omega} = \frac{1 - B1}{1 + B1} \tag{4}$$

where Y_0 is the coaxial admittance $= \frac{1}{Z0}$ with $Z0 = 50\,\Omega$ and $B1 = jC_0Z_0\omega$

The reflection coefficient S11 at the surface of the probe in contact with a material (of permittivity ε) is defined by:

$$\boldsymbol{S_{11s} = \frac{Y_0 - Y}{Y_0 + Y} = \frac{1 - jC_0Z_0\omega\varepsilon^b}{1 + jC_0Z_0\omega\varepsilon^b} = B2} \tag{5}$$

where Y_0 is the coaxial admittance $= \frac{1}{Z0}$ with $Z0 = 50\,\Omega$.

The reflection coefficient S11 (magnitude and phase) measurement was performed using a Vector Network Analyzer (ANRITSU 37325A). At the plane position P1 (Fig. 1), S11 can be expressed as:

$$s_{11}(P1) = \eta.\exp(i.\alpha) \tag{6}$$

where η is the magnitude of S11 and α the phase.

At the plane position P2, S11 is defined by:

$$s_{11}(P2) = \eta.\exp(i.\alpha).\exp(i4\pi d/\lambda) \tag{7}$$

where d is the electric length of the probe and λ is the wavelength.

Only S11(P2) can be measured. The parameter d is difficult to compute. Therefore, at the beginning of a measurement series, a measurement was performed without a sample (in the air). Then each measurement was normalized based on this value to remove the $\exp(i4\pi d/\lambda)$ term from the S11(P2) expression. We thus obtain:

$$\frac{S_{11}sample\,(P2)}{S_{11}empty\,(P2)} = \frac{S_{11}sample\,(P1)}{S_{11}empty\,(P1)} = \frac{S_{11s}}{S_{11e}} \tag{8}$$

So we can write:

$$\frac{S_{11}sample\,(P1)}{S_{11}empty\,(P1)} = \rho.\exp\left(j.\phi\right) \tag{9}$$

where ρ and φ can be obtained from S11 measurements performed at plane P2 with and without a sample.

From Eqs. (8) and (9) we obtain:

$$S_{11s} = \rho.\exp\left(j.\phi\right).S_{11e} = \rho.\exp\left(j.\phi\right).\frac{1 - B1}{1 + B1} = B2 \tag{10}$$

and from Eq. (5) we obtain:

$$B2 = \frac{1 - B1\varepsilon^b}{1 + B1\varepsilon^b} \tag{11}$$

Then Eq. (11) gives:

$$\varepsilon^b = \left(\frac{1 - B2}{1 + B2}\right).\frac{1}{B1} = A.\exp(j.\theta) \tag{12}$$

where A and θ are respectively the magnitude and the argument of the expression for ε^b.

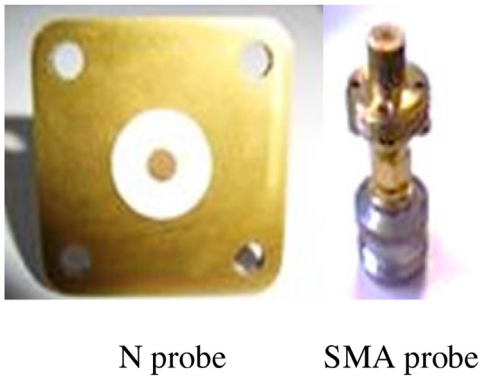

Fig. 2. Photographs of N probe and SMA probe.

Finally, from Eq. (12) we can compute the real and imaginary parts of the relative permittivity of the material:

$$\varepsilon = \sqrt[b]{A}.\exp\left(j.\frac{\theta}{b}\right) = \varepsilon' + j.\varepsilon' \tag{13}$$

This expression was used to compute the permittivity for each frequency.

The advantage of the method is its large frequency range (from 500 MHz up to 6 GHz for the SMA probe and from 500 MHz to 3 GHz for the N probe). The range depends on the shape and size of the probe.

This method also has some disadvantages. The small volume of the soil considered, because of the small penetration depth of waves (~1 cm) inside the sample, limits this technique to measurements of localized homogeneous media. The small penetration depth is mainly due to the propagation break at the end of the probe, which leads to the apparition of an evanescent wave (*i.e.* a wave tending to vanish because its intensity decays exponentially with the penetration in the media) in the material. A very good contact between the probe and the sample is required, making this technique well suited to solid samples with flat surfaces. If the magnitude of the S11 coefficient is too weak, there are errors due to noise interferences. If the value of the measured S11 for the sample is too close to the one measured for air, the dynamic measurement range is relatively small and the computation of the permittivity can be erroneous.

Nevertheless, if the above warnings are taken into consideration, it is possible to make accurate measurements. Furthermore, we designed probes with two different shapes. These shapes have been defined to ensure a good contact between the probe and the sample. For that purpose, we developed a Finite Element Method model of each probe as the results obtained with numerical computations were in good agreement with experiments. This approach allowed the development of two probes, named SMA and N probes to indicate the types of connector used (Fig. 2). As an example, Fig. 3 presents a comparison between numerical computations and measurements on wood samples. The fluctuations observed in the measurements were due to the imperfect contact between the probe and the sample for the experimental measurements, and the impedance mismatch between the probe, the coaxial cable and the network analyzer (which did not exist in the FEM computation).

2.2. Weak perturbation method

The results obtained with the end effect probes were compared to those obtained with the weak perturbation method [1] using a resonant cavity (RC). The latter is a rectangular waveguide made of Dural material (aluminum and copper alloy) closed at each extremity by a short circuit (Dural plate). The dimensions of the cavity are 0.165 m × 0.082 m × 0.514 m (width, height, length).

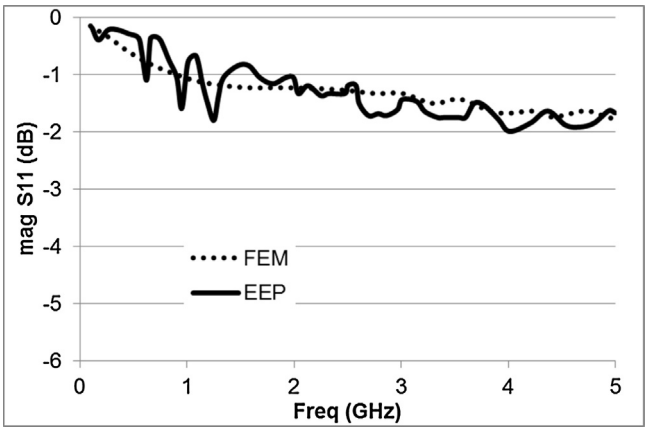

Fig. 3. Comparison between experimental results (EEP) and FEM computation for end effect probe.

Two antennas are connected to the cavity to generate electromagnetic (EM) waves within it. Each antenna is connected to a network analyzer by means of a coaxial cable. They are placed at a quarter wavelength from each Dural plate (*i.e.* a wavelength corresponding to the resonant frequency needed). Therefore, an EM stationary wave with $TE_{1,0}$ mode (*i.e.* Transverse Electric linked to the electromagnetic field distribution) resonates within the empty cavity. For Transverse Electric mode, the electric field is perpendicular to the direction of propagation. In the cavity, the electric field is parallel with the antennas which are connected to the network analyzer through coaxial waveguides. The transmission of EM waves from one antenna to the other through the cavity is possible at some resonant frequencies linked to the cavity dimensions. $TE_{1,0,3}$ mode is currently used (1, 0, 3 are the numbers of half wavelength variations of the electric field in the width, height and length directions respectively). The maximum magnitude of the electric field appears at the center of the cavity.

The resonance characteristics are f_0 (frequency) and Q_0 (quality factor).

The resonant frequency of an empty TE_{mnp} mode rectangular waveguide is given by:

$$f_{mnp} = \sqrt{\frac{c}{2}\left[\frac{m^2}{a} + \frac{n^2}{b} + \frac{p^2}{l}\right]} \tag{14}$$

with c the velocity of light and a, b, l the width, height and length of the cavity.

In our case, the resonant frequency f0 was 1.26 GHz.

Coupling effects between the cavity and the coaxial cables (*via* the antenna) are not taken into account in the previous relation.

The quality factor Q0 is defined by:

$$Q = 2\pi f \frac{Energy\ stored\ in\ the\ cavity}{Energy\ dissipated\ per\ cycle} = 2\pi f \frac{W}{\left(\frac{W}{dt}\right)} \tag{15}$$

with f the resonant frequency of the cavity and W the energy stored in the cavity

The denominator in Eq. (15) expresses the energy dissipated in the cavity. Such dissipation happens mainly in the sample.

The principle of this measurement technique relies on the link between the changes of the resonance parameters (f_1 and Q_1 resonant frequency and quality factor with sample) due to the introduction of a sample within the cavity and the dielectric properties of the sample.

The frequencies and the quality factors were obtained directly from the measurements of the complex transmission coefficient S21 with a network analyzer (ANRITSU 37325A). Before the measurements, a procedure to reduce errors was used to calibrate the

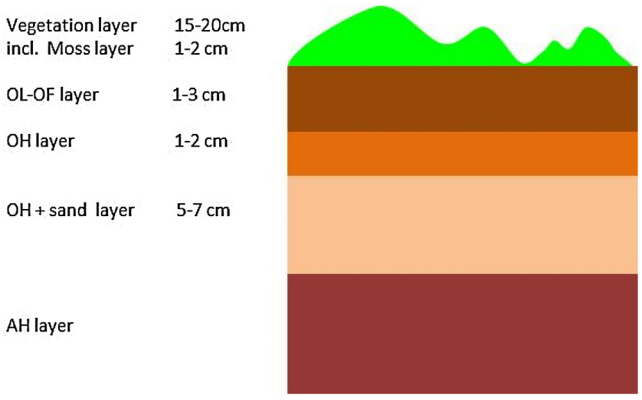

Fig. 4. Organic soil profile description.

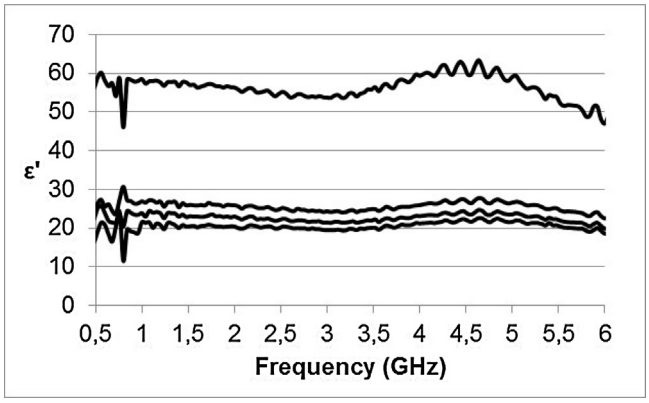

Fig. 5. Real part of the permittivity measured at OL-OF surface position using SMA probe. The four black lines represent four consecutive measurements where the probe was lifted and replaced each time.

network analyzer. Each measurement was repeated three times to ensure repeatability of the measurements and to minimize errors.

It has been shown [1] that the real (ε') and imaginary (ε") parts of the relative permittivity were then calculated as:

$$\varepsilon'_r = 1 + \frac{1}{\alpha} \times \frac{f_0 - f_1}{f_0}$$
$$\varepsilon''_r = \frac{1}{2\alpha}\left(\frac{1}{Q_1} - \frac{1}{Q_0}\right) \quad (16)$$

where α is the filling factor. As a first approximation it can be estimated using:

$$\alpha = 2.\frac{sample\ volume}{cavity\ volume} \quad (17)$$

In order to improve the accuracy of the permittivity estimation, the coefficient α can be estimated from measurements on well-known materials (*e.g.*, water, polytetrafluoroethene PTFE). In this study, water samples were used to define this parameter.

The weak perturbation method is a very accurate technique. Unfortunately, it allows the measurement to be made at only one frequency (the resonance frequency) and it is a laboratory technique that is not suitable for *in situ* measurements.

2.3. Preparation of organic soil samples and measurement protocol

The measurements presented in this study were made using organic soil collected in the framework of the SMOSHiLat project. The material included the organic soil layers (OL OF OH) and the top part of the underlying sandy mineral AH layer and originated from heathland within the Gludsted Plantation, situated in the Skjern River Catchment, Denmark. Soil excavation was undertaken with support from the Danish HOBE project ([20], www.hobe.dk).

A geometric representation of the soil profile is presented in Fig. 4.

The soil system is overlaid by a vegetation layer (mainly Scotch heather grass and moss). In this study, we focused our investigations on the permittivity measurement of organic soil layers. To describe the samples, we used a classification developed by the European Humus Forms Reference Base [21]. All organic horizons were present, *i.e.* not/weakly decomposed "litter" (OL), semi-decomposed "fragmented" matter (OF), and well-decomposed "humus" (OH). However, as the OL and OF layers were thin and it was not easy to distinguish between them, they were treated as a unit (OL-OF) and since, for the present type of humus, a sharp transition between the OH and the underlying mineral (sand) layer was typically absent, the lowest part of the sample was considered as a mixture of the two (OH + AH sand layer).

Measurements were made in the IMS laboratory (Integration from Material to System Laboratory Bordeaux University, France), at room temperature (20 °C), using a soil sample with dimensions of approximately 15 cm × 15 cm × 15 cm.

The measurements were performed with the two end effect probes (N and SMA probes) successively. The probes were connected to a Vector Network Analyzer (VNA, ANRITSU MS2026A) for the S11 coefficient measurements. The probes were placed at four different depths: at the surface of the organic soil structure (OL-OF surface measurement), 2 cm deep within the OL-OF layer, within the OH layer and finally in the OH + sand layer.

For each depth, the measurements were repeated four times in succession to avoid erroneous data due to poor placement of the probe. A wrong position of the probe could be easily identified because it induced abnormally low permittivity (real part of the permittivity measured limited to the range [1;2] due to a thin film of air between the probe and the soil surface) or abnormally high permittivity (real part of the permittivity measured greater than 60 due to a film of water if too much pressure was applied to the probe). If one of the measurements deviated markedly from the others (see Fig. 5 for an example) it was detected visually and discarded to keep the reliable data. An average value was computed using only the reliable measurements.

The samples collected have been stored in the laboratory so they dried partially at room temperature. Before the measurement process, all samples were gradually watered from the top.

Once the dielectric measurements had been carried out, samples of the different layers were collected. To obtain the water contents, the soil samples were dried for three days (72 h) at 80 °C. O'Kelly [22] estimated that, around this temperature, the mass loss due to charring balanced the effects of residual water caused by the strong water binding capacities of organic matter.

In this study, the classical method for determining soil moisture content was used. Volumetric soil moisture (SM) was computed as:

$$SM = \frac{W_W}{W_{Dry}}\rho_b \quad (18)$$

where

W_W is the weight of water in the sample (g),

W_{Dry} is the weight of the dry sample (g) and ρ_b is the soil bulk density (g/cm3).

The water contents obtained at each depth are presented in Table 1.

Table 1
Sample moisture content at each depth.

Probe position	Moisture (m^3/m^3)
OL-OF surface	0.40
OL-OF	0.58
OH	0.72
OH + sand	0.50

2.4. Measurement errors

There are several possible causes for errors occurring during the measurement of the soil permittivity. They can be related to the weighing of the sample, the methods of measurement and calculation of the permittivity, or the sample heterogeneity. These different sources of errors have been analyzed and discussed by Demontoux et al. [23]. We can classify the errors in two main groups:

2.4.1. Instrumental errors

The calibration of the vector network analyzer corrects for some random and intrinsic imperfections of the apparatus. The latter are due to errors in the measurement of the standards, degradation of the signal0to-noise ratio (interfering signals), various drifts (thermal, atmospheric and electronic) or connection errors. Further uncertainties can be caused by rounding approximations during numerical calculations. These two types of error are difficult to quantify but we estimated their influence on the measurement results to be lower than 5%.

2.4.2. Calculation errors in the sample weighing

The error in the calculation of the moisture content was mainly due to errors in sample weighing. The standard deviation of the measured values was ±0.05 g.

The maximum uncertainty of a function y with several variables x, z is calculated in the following way:

$$\begin{cases} y = f(x,z) \\ \Delta y = |\frac{\partial f}{\partial x}|\Delta x + |\frac{\partial f}{\partial z}|\Delta z \end{cases} \quad (19)$$

It then follows from Eq. (18) that:

$$\Delta SM = |\frac{SM}{W_W}|\Delta W_W + |\frac{SM}{W_{Dry}}|\Delta W_{Dry} \quad (20)$$

For the soil, the moisture content is computed after weighting samples collected on the soil blocks used. Taking into account the measurements considered in this study, we obtain the following ranges for each variable:

$$\text{Soil}: \begin{cases} 0 \le SM \le 0.72 \\ 0 \le W_W \le 108g \\ 0 \le W_{Dry} \le 31g \end{cases}$$

We assume an error of ±0.10 g on the weights, because the water and dry weights are calculated, respectively, by differences between the wet and dry weights, and between the weight of the sample and the support and the weight of the support alone.

We computed an error in the soil moisture estimation of ±0.29% [23].

When concrete slabs are wetted, water may penetrate into the interstitial voids of the material (*i.e.* pores).

When all the pores in a concrete are filled with water, it is defined as saturated. The degree of saturation is the ratio of pore volume filled with water and the total volume. It can also be calculated from the volumetric moisture content. There is no error to compute in saturation determination in our experiments because we studied 0% and 100% of saturation.

Table 2
C_0 and b values for the probes.

Parameters	SMA probe	N probe
b	1.05	1.2
C0	9.10^{-15}	3.10^{-14}

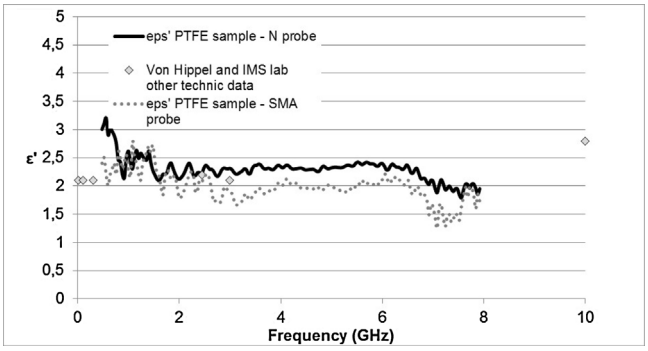

Fig. 6. N and SMA probes (ε') measurements versus resonant cavity and Von Hippel's (Von Hippel et al., 1960) measurements – Material: PTFE.

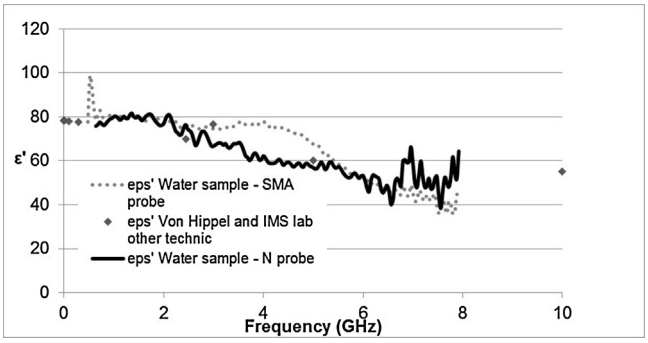

Fig. 7. N and SMA probe (ε') measurements compared with resonant cavity and Von Hippel's measurements – Material: water.

3. Results

3.1. Estimation of the probe parameters

Measurements were made on water and polytetrafluoroethylene (PTFE) to calibrate the parameters C0 and b of each probe. These parameters depend on the measurement frequency and on the permittivity of the samples.

To simplify the data processing, we used a common value of these parameters over the whole frequency and permittivity ranges (Table 2).

Fig. 6 presents the real part of the permittivity measurements obtained with a PTFE sample using the two probes (N and SMA). Good agreement can be seen between probe measurements and other data (literature and resonant cavity measurements). All the imaginary part values of the permittivity measurements performed (probes and resonant cavity) were small, falling within the range [0.01;0.05], which is close to the assumed measurement error. So the curves are not represented. The average value obtained was observed to be in agreement with the data found in the literature (Von Hippel et al. [24]).

Figs. 7 and 8 present the real and imaginary part of permittivity measurements obtained for water taken with both probes (N and SMA) compared with data obtained from resonant cavity

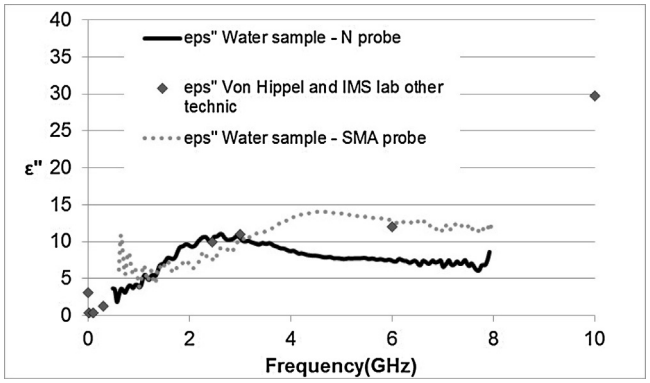

Fig. 8. N and SMA probe (ε") measurements compared with resonant cavity and Von Hippel's measurements – Material: water.

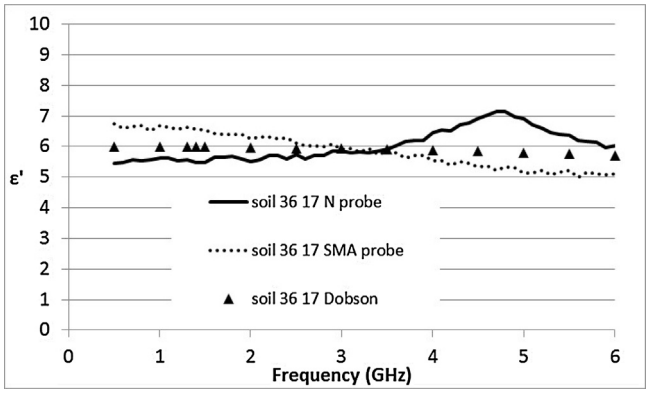

Fig. 9. N and SMA probes (ε') measurements versus Dobson model – Material: soil 36% sand 17% Clay.

Table 3
Soil characteristics as measured by the INRA laboratory of Arras.

Clay (g/kg)	166
Fine silt (g/kg)	288
Coarse silt (g/kg)	186
Fine sand (g/kg)	230
Coarse sand (g/kg)	130
P_2O_5 (g/kg)	0.019
MgO (g/kg)	0.14
K_2O (g/kg)	0.07
$CaCO_3$	<1 g/kg
Organic carbon (g/kg)	8.36
Organic matter (g/kg)	14.4
Organic nitrogen (g/kg)	1.03

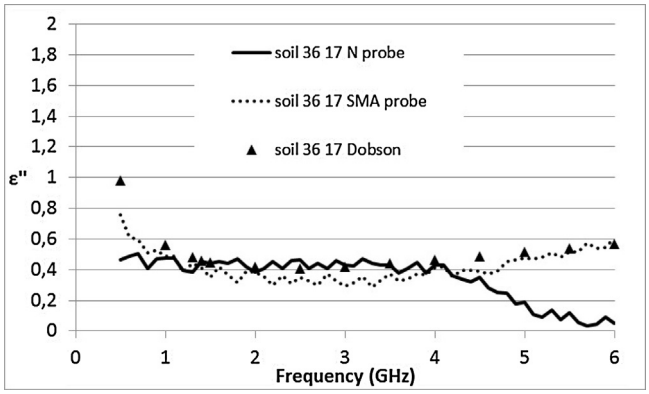

Fig. 10. N and SMA probes (ε") measurements versus Dobson model – Material: soil 36% sand 17% Clay.

measurements or in the literature. On Figs. 6–8, a variance can be observed, which depends on the probe used and the frequency. We conclude that the two probes have different frequency ranges. For the N probe, the maximum range is [500 MHz; 3.5 GHz] and for the SMA probe it is [500 MHz; 6 GHz]. In this paper, considering the values of C0 and b chosen and the range of permittivities encountered, the upper frequency measurement was limited to 3.5 GHz for the N probe and 6 GHz for the SMA probe. So, although the results for the N probe measurements are presented over a larger frequency range, we will discuss them only over the frequency range [500 MHz; 3.5 GHz].

Within these frequency spectra, the end effect probe measurements on well-known materials (water, PTFE) coincide with other measurements (resonant cavity (RC) method and Von Hippel's method (Von Hippel et al. [24]). However, with the example of the measurements on the organic soil samples presented below we will demonstrate that the upper frequency limit decreases with increasing permittivity.

3.2. Measurements on mineral soil and concrete

Firstly, the permittivity was evaluated with end effect probes using mineral soil and concrete media.

3.2.1. Mineral soil

The soil collected was analyzed. It contained 36% sand and 17% clay (details in Table 3). The soil block collected was 15 cm × 15 cm × 20 cm (length, width, height respectively). Before the dielectric measurements were carried out, the soil block was dried for one day (24 h) at 105 °C. This protocol was specifically designed not to damage (scorch mark. . .) the mineral soil material [19] [23]. Then the sample was moistened from the top. After the dielectric measurements on the top layer, a sample was collected from the top layer studied. This sample was weighed and dried, and the moisture content was computed from the change in weight. We found a moisture content of 0.104 (m3/m3).

Figs. 9 and 10 present the mineral soil dielectric measurements (respectively the real part of the permittivity, ε', and the imaginary part of the permittivity, ε") obtained with N and SMA probes. The permittivity measurements of the soil were compared with the permittivity estimations computed using the Dobson model [5,6].

Concerning ε', the End Effect Probe (N and SMA) measurements are in agreement with the ε' values computed using the Dobson model over the whole frequency range of the study [500 MHz; 6 GHz].

In the case of ε", the results show very good agreement over the whole frequency range [500 MHz;6 GHz] for the SMA probe. For the N probe, the agreement with the Dobson model estimations is limited to frequencies lower than 4.5 GHz.

3.2.2. Concrete

The measurements were carried out on a concrete slab of dimensions 21 cm × 28 cm × 7 cm. They are placed on one face of the concrete block. The concrete was a class 30 MPa cast with 400 kg/m^3 of CEM II 32.5 R cement. Aggregates were siliceous rolled gravel and sand with sizes of about 0–12.5 mm. Due to the small penetration depth of the electromagnetic wave emitted by the probes (~1 cm) and the depth at which the aggregates were found; we concluded that the probe measurements were not impacted by the aggregates.

After 28 days, the slabs were conditioned to have a uniform moisture distribution of about 0% or 100% saturation of the material.

The 0% moisture slab was dried in an oven at 70 °C until the mass had stabilized (approximately 1 month). The 100% slab was

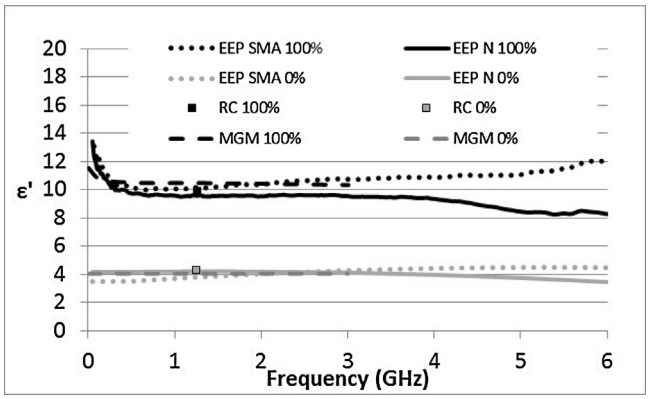

Fig. 11. N and SMA probe (ε') measurements compared with resonant cavity measurement – Material: concrete – Moisture saturation: 0% and 100%.

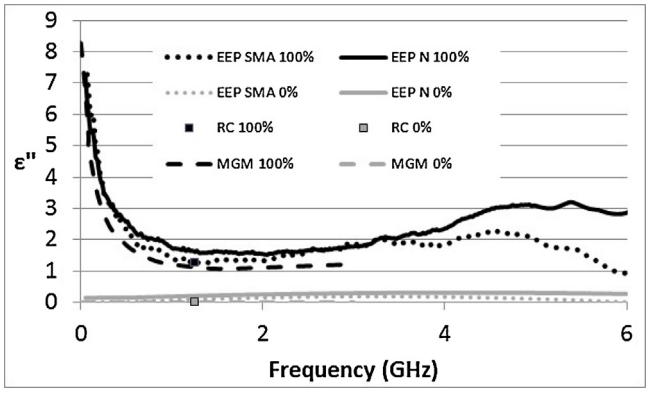

Fig. 12. N and SMA probe (ε") measurements compared with resonant cavity measurement – Material: concrete – Moisture saturation: 0% and 100%.

placed in water to reach full moisture saturation. In order to achieve homogeneous moisture distribution throughout the concrete volume, the samples were sealed with a plastic film and a layer of aluminum paper to preserve the saturation state and after stored in an oven at 70 °C for at least 2 weeks.

Figs. 11 and 12 present the real and imaginary part of permittivity measurements obtained for concrete made with both probes (N and SMA) compared with data obtained by the resonant cavity measurement (1.26 GHz) and the analytical dielectric model [25,26]. This dielectric model (referenced as MGM in this paper) allowed concrete permittivities from 0 to 3 GHz to be estimated.

We observe good agreement between the probe and the cavity measurements for both the real and the imaginary part of the permittivity.

There is a slight difference between probes measurement and dielectric model computation for imaginary part up to 3 GHz and good agreement for the real part.

For frequencies from 3 GHz up to 6 GHz, probe measurements of imaginary part increase which is not expected for concrete. This deflection is greater for the N probe and would be attenuated for the SMA probe if we introduced the frequency dependence of probe parameters.

This discrepancy between N and SMA measurements for frequencies greater than 3.5 GHz confirms the limit of N probes for measurements at the highest frequencies.

3.2.3. Organic soil measurements

3.2.3.1. OL OF surface measurements. Figs. 13 and 14 present the real and imaginary parts of the relative permittivity corresponding to the OL-OF surface position for both SMA and N probes. Values

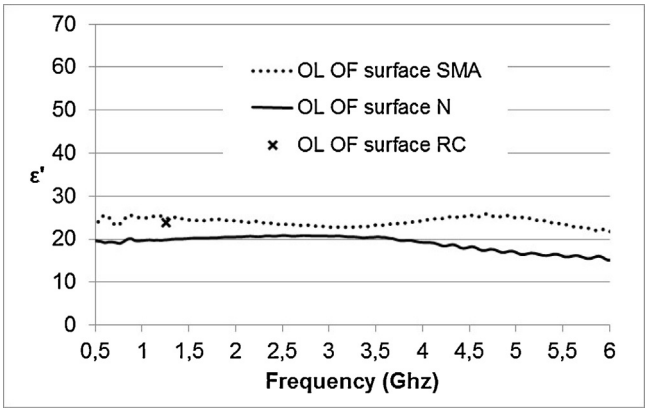

Fig. 13. Real part of the permittivity – OL OF surface position – from SMA and N probes and RC measurements.

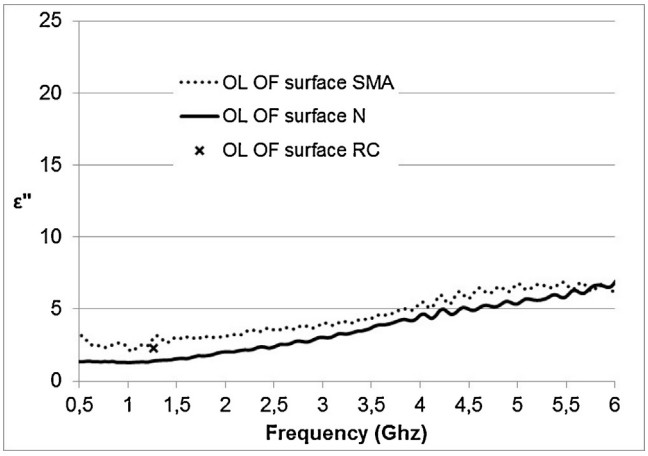

Fig. 14. Imaginary part of the permittivity – OL OF surface position – SMA and N probes, resonant cavity measurement.

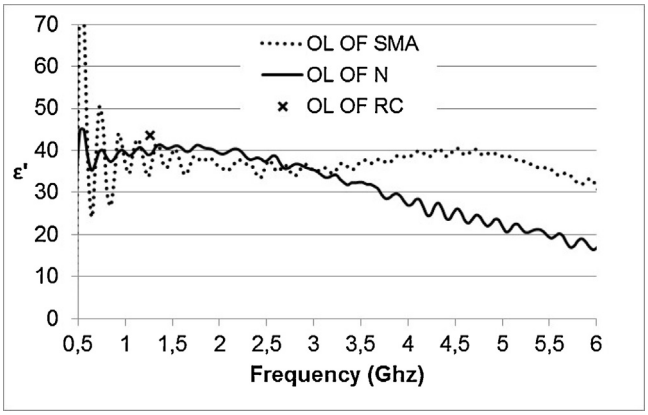

Fig. 15. Real part of the permittivity – OL OF position – from SMA and N probes, and RC measurements.

of the real permittivity vary between 15 and 25 for frequencies up to 6 GHz. The imaginary part increases with frequency from 0 to 6 GHz, with values varying from 2 to 7. The measurements made by the two probes are in good agreement with each other and with the RC measurements at 1.26 GHz.

3.2.3.2. OL OF layer measurements. Figs. 15 and 16 present the real and imaginary parts of the relative permittivity corresponding to the OL-OF position (at 2 cm depth) for both SMA and N probes.

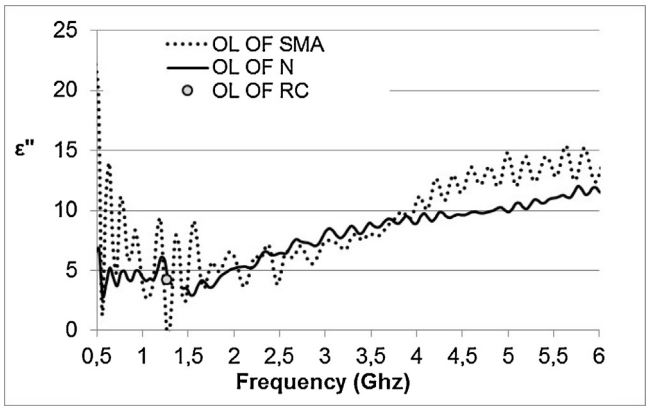

Fig. 16. Imaginary part of the permittivity – OL OF position – from SMA and N probes, and RC measurements.

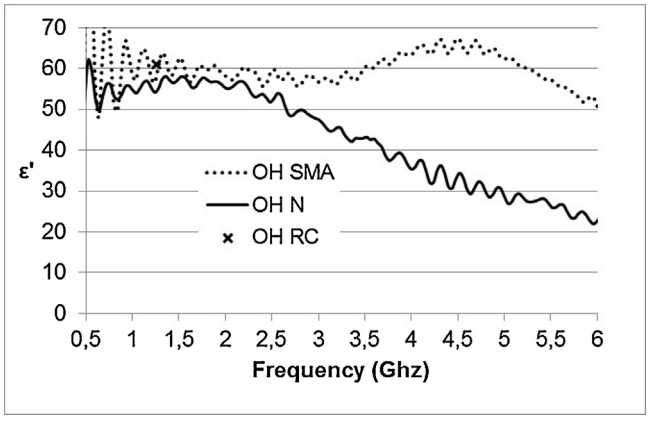

Fig. 17. Real part of the permittivity – OH position – from SMA and N probe, and RC measurements.

Considerable oscillations can be observed at very low frequencies concerning measurements with the SMA probe for both real and imaginary parts. Real permittivity varies between 20 and 45 for frequencies up to 6 GHz. Except for oscillations at low frequency, the imaginary part increases with frequency from 0 to 6 GHz with values varying from 4 to 15. The measurements made with the two probes are comparable with each other up to 3.5 GHz and with the RC measurements at 1.26 GHz.

3.2.3.3. OH layer measurements. Figs. 17 and 18 present the real and imaginary parts of the relative permittivity corresponding to the OH position for both SMA and N probes. Again, oscillations are more distinct for the SMA probe measurements at small frequencies for both real and imaginary parts. Values of the real permittivity measured with the SMA and N probes are comparable up to 3.5 GHz, with values varying between 50 and 60. Between 3.5 and 6 GHz, values of the real permittivity measured with the N probe decrease to 20 while those measured with the SMA probe stay around 60. Except for the oscillations, the imaginary part of the permittivity increases from 0 to 6 GHz. The measurements made with the two probes are in good agreement up to 3.5 GHz, with values varying from 5 to 13. Between 3.5 and 6 GHz, the imaginary part measured with the N probe stabilizes around a value of 13 while the value measured with the SMA probe increases to 20. The measurements with the two probes are in good agreement with the RC measurements at 1.26 GHz.

3.2.3.4. OH and AH sand layer measurements. Figs. 19 and 20 present the real and imaginary parts of the relative permittivity corresponding to the OH and AH sand layer for both SMA and N probe measurements. More oscillations are visible in the SMA probe measurements of both the real and imaginary parts, especially at low frequencies. Values of the real permittivity measured with the SMA and N probes are in good agreement up to 3.5 GHz, with values close to 50. Between 3.5 and 6 GHz, the values of the real permittivity measured with the N probe decrease to 25 while those measured with the SMA probe vary around 50. Except for the oscillations,

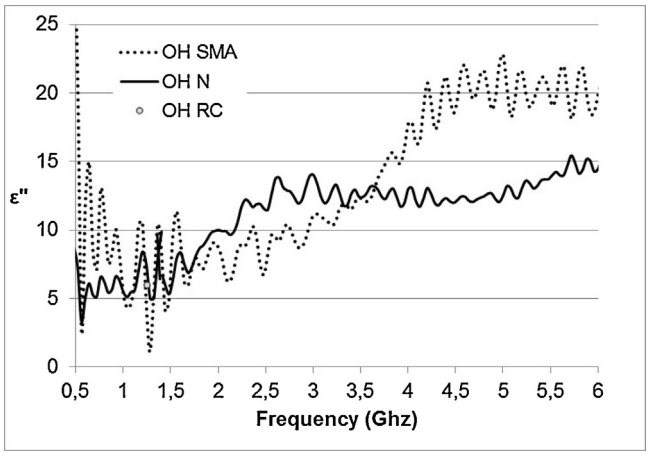

Fig. 18. Imaginary part of the permittivity – OH position – from SMA and N probe, and RC measurements.

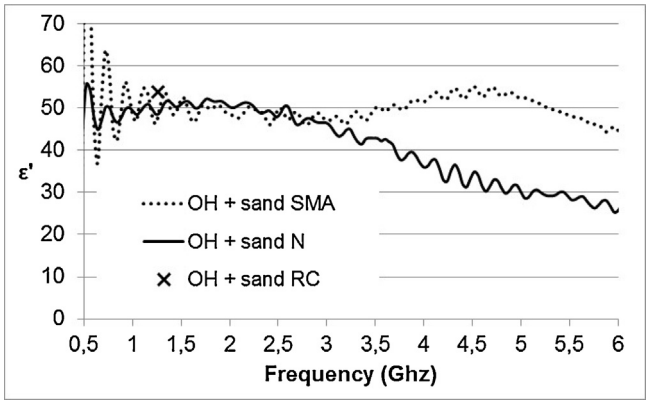

Fig. 19. Real part of the permittivity – OH + AH sand position – from SMA and N probes, and RC measurements.

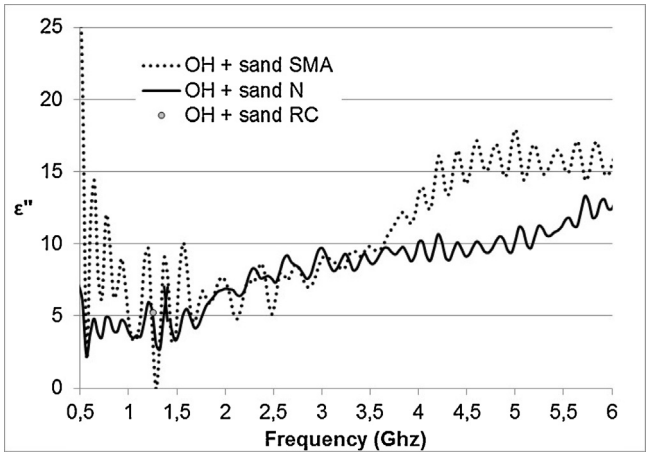

Fig. 20. Imaginary part of the permittivity – OH + AH sand position – from SMA and N probes, and RC measurements.

Table 4
N probe upper frequency limit at each depth.

Probe position	Moisture (m^3/m^3)	Upper frequency limit (GHz)
OL-OF surface	0.40	6
OL-OF	0.58	3.8
OH	0.72	3.5
OH + AH sand	0.50	3.5

the imaginary part of the sample permittivity increases with frequency from 0 to 6 GHz. The two probes present measurements in good agreement up to 3.5 GHz, with values varying from 5 to 10. Between 3.5 and 6 GHz, values of the imaginary part measured with the N probe increase slightly to 12 while those measured with the SMA probe increase to 15 and stabilize between 4 and 6 GHz. Except for the oscillations, the measurements with the two probes are in good agreement with the RC measurements at 1.26 GHz.

4. Discussion

The study based on measurements on water and PTFE samples showed that the frequencies up to which the methods were valid were ≈3.5 GHz for the N probe and ≈6 GHz for the SMA probe.

Measurements performed on concrete and mineral soil confirmed the validity domain of the end effect probes used. Nevertheless, the latter showed that the measurement frequency range could be extended to [100 kHz;6 GHz] in the case of homogeneous, slightly rough samples.

The measurements performed on organic soils showed that these values of the frequency range varied with the permittivity of the sample in the case of the N probe (Table 4). Nevertheless, we assume that a frequency range of [0.5 GHz; 3.5Ghz] for the N probe allows accurate measurement.

The higher the permittivity values were, the higher were the oscillations of the measurements. In contrast, the lower the frequency, the higher the oscillations. This was mainly due to the strong reflection at the boundary between the probe and the sample and to the reflection at the cable/probe interface.

While the valid frequency range for the N probe was more restricted than that of the SMA probe, the oscillations were found to be smaller for the N probe measurements than for the SMA probe measurements. This effect was mainly due to the greater size of the N probe compared to the SMA probe, which resulted in a more stable contact between the probe and the sample for the N probe.

Nevertheless, we observed good overall agreement among measurements made with the N probe, the SMA probe and the RC method. Furthermore, we observed clear trends in the shapes of the curves and a trend line, filtering out the oscillations, could be easily computed (Fig. 21).

Overall, we observed that the real and imaginary parts of the permittivity measured at all four sample depths were almost constant between 500 MHz and 1.5 GHz. At the same time, for both the SMA and N probes, we found that the real part was still almost constant up to 3 and 6 GHz, whereas the imaginary part increased between 1.5 GHz and 6 GHz. The magnitude of this increase was found to depend on the moisture content and on the type of layer considered. The largest increase was obtained for the OH layer at a soil moisture of 0.72 m^3/m^3.

As an example, Tables 5 and 6 present results obtained with both probes on the OL-OF layer at different frequencies and different moisture contents.

5. Conclusion

The study based on measurements on water and PTFE samples showed good agreement with probe measurements. The frequency limits up to which the methods were valid depend on the probe type and the permittivity of the sample measured. These limits appear to be ≈3.5 GHz and ≈6 GHz for the N probe and the SMA probe respectively. These limits were confirmed by measurements on concrete and mineral soil.

By complying with a specific measurement protocol (position of the probe, study and selection of the measurements, use of mean value over various measurements) and in spite of oscillations, in particular in the case of the SMA probe, we obtained consistent data in the case of measurements on organic soil. Furthermore, in the case of organic soil measurements, SMA and N probe measurements were very close and corresponded to RC measurements. The oscillations observed are mainly due to the not yet ideal contact between the probe and the material under investigation and depend on the media studied (interaction surface, heterogeneities. . .). They occur especially at low frequency. Studies are carried out to modify the tip of the probes (especially the SMA probe) to improve the probe-material contact and to avoid the oscillations observed.

We have shown that end effect probes are efficient for *in situ* dielectric measurements over a wide range of frequencies on different materials and different sample structures (with a more or less rough interface).

We have identified parameters that can optimize the end effect probes, such as the coaxial connector used or the interface surface. The SMA format of the probes allows measurements to be made at higher frequencies than the N format. The N format limits the measurement oscillations for low frequencies.

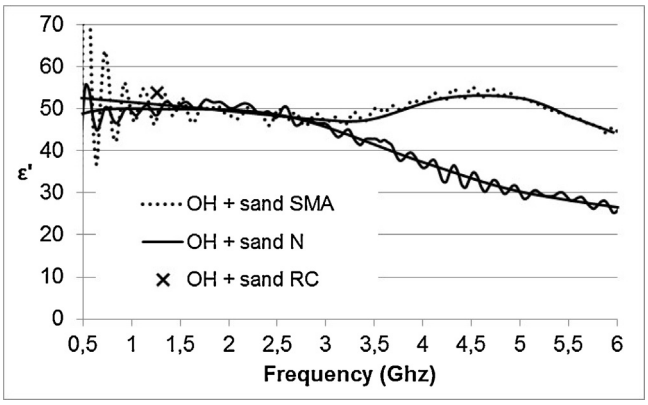

Fig. 21. Trend line – Real part of the permittivity – OH + sand position – SMA and N probe, RC measurement.

Table 5
real part of the relative permittivity measurements made with SMA and N probes at different frequencies and moisture contents at OL-OF layer.

Moisture	1 GHz	1.4 GHz	3 GHz	5 GHz	probe
0.4	19.67	20.06	20.74	16.9	N
0.58	35.6	36.6	34.3	21.96	N
0.4	25.07	24.9	22.93	25.05	SMA
0.58	36.42	36.67	35.16	38.67	SMA

Table 6
Imaginary part of the relative permittivity measurements made with SMA and N probes at different frequencies and moisture contents at the OL-OF layer.

Moisture	1 GHz	1.4 GHz	3 GHz	5 GHz	probe
0.4	1.76	2	4.17	7.24	N
0.58	4	3.78	7.73	10.21	N
0.4	2.24	2.66	4.04	6.78	SMA
0.58	3.93	5	7.45	14.8	SMA

Further work will enable a new end effect probe to be developed, combining the advantages of the two probes (frequency range of SMA probe, better probe-material contact of N probe, low oscillation measurement of N probe). The final objective is to develop reliable stand alone probes for *in-situ* permittivity measurement.

Funding

This work was supported by the French National Centre for Space Studies (CNES) in the framework of TOSCA SMOS project.

References

[1] Boudouris, Validité de la méthode de perturbation appliquée aux cavités résonnantes pour la mesure de la perméabilité et de la permittivité des petits échantillons, Annales Télécommunications 19 (1964) 63–80.
[2] F. Demontoux, Contribution à l'amélioration des mesures de permittivité à 2450MHZ et au développement d'un applicateur micro ondes dédié à la flash pasteurisation à l'aide de modélisations électromagnétique et thermique, University Bordeaux PhD (1999).
[3] W.B. Weir, Automatic measurement of complex dielctric constant and permeability at microwave frequency, Proceedings of IEEE 62 (1974) 33–36 (no%11).
[4] F. Demontoux, B. Le Crom, G. Ruffie, J. Wigneron, J.V. Grant et Mironov, Electromagnetic characterization of soil-litter media: application to the simulation of the microwave emissivity of the ground surface in forests, Eur. Phys. J. Appl. Phys. 44 (%13) (2008) 303–315.
[5] M.C. Dobson, F.T. Ulaby, M.T. Hallikainen, M.A. El Raves, Microwave Dielectric Behavior of Wet Soil-Part II: Dielectric Mixing, IEEE Trans. Geosci. Remote Sens. %1 sur%2GE-23 (%11) (1985) 35–46.
[6] M.C. Dobson, F.T. Ulaby, M.T. Hallikainen, et al., Observations, microwave dielectric behavior of wet soil-part I: empirical models and experimental observations, IEEE Trans. Geosci. Remmote Sens. 23 (%11) (1985) 25–34.
[7] V. Mironov, Y. Kerr, J.P. Wigneron, L. Kosolapova, F. Demontoux, Temperature- and texture-dependent dielectric model for moist soils at 1.4 GHz, IEEE Geosci. Remote Sens. Lett. 10 (% 13) (2013) 419–423.
[8] B. Rao, A. Bhat, D. Singh, Application of impedance spectroscopy for modeling flow of AC in soils, Geomach. Geoeng. Int. J. 2 (%13) (2007) 197–206.
[9] A. Bhat, B. Rao, D. Singh, A generalized relatinship for estimating dielectric constant of soils, J. ASTM Int. %1 sur%2 (2007), http://dx.doi.org/10.1520/JAI100635 (p. 12).
[10] K. Rohini, D. Singh, A methodology for determination of Electrical Propertiees of Soils, J. Testing Eval. ASTM 32 (%11) (2004) 64–70.
[11] Decagon Devices Inc,ECH20 Soil Moisture Sensor, Operator's manual for model 5TE. Decagon Devices Inc., 2365 NE Hopkins Court, Pullman, WA 99163, USA, (2014).
[12] Delta T devices Ltd, ThetaProbe Soil Moisture sensor Type ML2x user Manual ML2x-UM-1.21. Delta-T Devices Ltd. 128 Low Road, Burwell, Cambridge CB5 0EJ, GB, 1999.
[13] Hanumantha, B. Rao, V. Sridhar, R. Rakesh, D. Sing, P. Narayan, P. Wattal, Lysimetric Studies fo modelling radioactive contaminant transport in soils, Int. J. Environ. Waste Manage. IJEWM 12 (%13) (2013) 318–339.
[14] S. Jones, J. Wraith, D. Or, Time domain reflectometry measurement principles and applications, Hydro Process 16 (2002) 141–153.
[15] S. Bircher, S. Razafindratsima, F. Demontoux, M. Andreasen, J. Vuollet, K. Rautiainen, F. Jonard, L. weihermüler, P. Richaume, A. Mialon, J.Y. Wigneron et Kerr, Soil Moisture and Dielectric constant measurements of organic soils in the higher northern latitudes in support of the SMOS mission, in: Transaction of the Fourth International Smposium on Soil Water Measurement Using Capacitance, Impedance and TDT, Montreal Canada July 16–18, 2014.
[16] ESA, ESA website: http://www.esa.int/esaLP/LPsmos.html, [En ligne].
[17] Y. Kerr, P. Waldteufel, et al., Soil moisture retrieval from space: the Soil Moisture and Ocean, IEEE Trans. Geosci. Remote Sens. 39 (%18) (2001) 1729–1735.
[18] J. wigneron, Y. Kerr, P. Waldteufel, L-band microwave emission of the biosphere (L-MEB) model, Remote Sens. Environ. 107 (2007) 639–655.
[19] M. Stuchly, S. Stuchly, Coaxial line reflection methods for measuring dielectric properties of biological substances at radio and microwave frequencies, IEEE Trans. Instrum. Meas. 29 (1980) 176–183.
[20] K. Jensen, T. Illangaskare, HOBE: a hydrological observatory, Vadose Zone J. 10 (2011) 1–7.
[21] A. Zanella, B. Jabiol, J. Ponge, G. Sartori, R. De Wall, B. Van Delft, U. Graefe, N. Cools, K. Katzensteiner, H. Hager, M. Englisch, A. Brethes, G. Broll, J. Gobat, J. Brun, G. Milbert, E. Kolb, U. Wolf, L. Frizzera, P. Galvan, R. Kolli, R. Baritz, R. Kemmers, A. Vacca, G. Serra, D. Banas, A. Garlato, S. Chersich, E. Klimo, R. Langohr, European Humus Forms Reference Base, http://hal.archives-ouvertes.fr/hal-00541496/ (2011).
[22] B. O'Kelly, Accurate determination of moisture content of organic soils using the oven drying method, Drying Technol. 22 (%17) (2004) 1767–1776.
[23] F. Demontoux, B. Le Crom, G. Ruffie, J. wigneron, J. Grant, V. Mironov, Electromagnetic characterization of soil-litter media – application to the simulation of the microwave emissivity of the ground surface in forests, Eur. Phys. J. Appl. Phys. 44 (%13) (2008) 303–315.
[24] V. Hippel, Dielectric Materials and Applications, The technology press of MIT, 1960.
[25] Z. Sbartai, C. Maï, F. Bos, S. Razafindratsima, F. Demontoux, Non destructive evaluation of timber structures using GPR technique, in: 15th International Conference on Ground Penetratin Radar (GPR 2014), Brussels, Belgium, June 30 July 4 2014, 2014.
[26] S. Matthews, A. Goodier, S. Massey, Permittivity measurements and analytical dielectric modeling of plain structural concrete, in: Proceedings of the Seventh International Conference on Ground Penetrating Radar, Laurence, Kansas USA, 1998, pp. 363–368.

Biographies

François Demontoux (M'09) received the Ph.D. degree in physics from the University of Bordeaux, Talence, France, in 1999. He is currently a Research Scientist with the IMS Laboratory, Bordeaux, France, where he has been the Head of the Electromagnetic Characterization and Remote Sensing (CEMT) Team until 2015. Currently he is with the MIM (Mirowave-Interaction-Materials) research team. He participated in the development of the forward model (L-MEB) for soil and vegetation in the ESA-SMOS mission level-2 retrieval algorithm. His research interests include microwave remote sensing of soil and vegetation, modeling of the electromagnetic phenomena, and electromagnetic characterization of materials.

Stephen Razafindratsima received his degree in Hydraulic Engineering from Ecole Polytechnique of Antananarivo, Madagascar in 2001; his M. Sc. degree in Hydrology, Hydrogeology, Geostatistics and Geochemistry from University of Pierre and Marie Curie, Paris, France in 2003; his Ph.D. degree in Geosciences from University of Pierre and Marie Curie Paris, France in 2007. He worked in Computer programming company for two years before joining Bordeaux as Teacher and Research Fellow in Geophysics in 2010. In 2011 he worked as Research Assistant in Nantes School of Mines, in Hydrogeological Modeling. In 2013, he joined IMS laboratory in Bordeaux to work for Electromagnetic characterization of organic soils and wood samples. Then he was Teacher in High Schools in Bordeaux before joining I2M laboratory in Bordeaux where he is doing research in Civil Engineering.

Simone Bircher (M'12) received the M.Sc. degree in geography from the University of Zurich (UZH), Switzerland, in 2007 and the Ph.D. degree from the Technical University of Denmark, Kongens Lyngby, Denmark, in 2012. She conducted research at the GIScience Center, UZH, and in the Division of Geodynamics, DTU Space Department, and joined different glaciological campaigns in the Arctic and Alps. During her PhD and a postdoc with the Department of Geography and Geology, University of Copenhagen, Denmark, her research focused on the validation of SMOS products in the scope of the Danish Hydrological Observatory (HOBE), including the establishment of long-term *in situ* measurements, and the organization of an airborne calibration/validation campaign. Currently, she is with the Centre d'Etudes Spatiales de la Biosphère, Toulouse, France. She is working on the calibration/validation of the SMOS soil moisture retrieval algorithm over high-latitude environments with particular focus on the characterization of microwave L-band emissions from organic-rich soils.

Gilles Ruffié receive the Ph.D degree in electronic from the University of Lille in 1987. He is now in charge of the dielectric characterization platform at IMS laboratory in Bordeaux. He manages projects on the application of Microwave on materials.

Fabrice Bonnaudin, received a MASTER degree in design and use of physical instrumentation of Bordeaux University in 2004. He is now an engineer at the dielectric characterization platform at IMS laboratory. He aims to improve technics for dielectric measurement of material.

François Jonard received the M.Sc. and Ph.D. degrees in bioengineering from the Université catholique de Louvain (UCL, Belgium), in 2002 and 2012, respectively. From 2003 to 2004, he worked at UCL as a Research Assistant on modeling water fluxes in forest ecosystems. From 2006 to 2009, he worked as a Project Manager in different consultancy companies in the fields of water resource management, geographic information systems and remote sensing of the environment. Since 2009, he has been with the Agrosphere, Institute of Bio- and Geosciences, Forschungszentrum Jülich GmbH (FZJ, Germany). In 2011, he spent several months at the NASA Goddard Space Flight Center (Greenbelt, MD) as a Visiting Scientist working in the context of the Soil Moisture Active and Passive (SMAP) mission. Since 2015, he has been an Associate Professor with the Faculty of Bioscience Engineering and the Earth and Life Institute (UCL) and a Research Associate with the Agrosphere (FZJ). His current research interests include hydrogeophysics and microwave remote sensing of soil and vegetation.

Jean-Pierre Wigneron (SM'03) received the M.Sc./Engineering degree from SupAéro, Ecole Nationale Supérieure de l'Aéronautique et de l'Espace (ENSAE), Toulouse, France, in 1987 and the Ph.D. degree from University of Toulouse, France, in 1993. He is currently a senior research scientist at the Institut National de Recherche Agronomiques (INRA), ISPA, Bordeaux, France, co-coordinator of remote sensing activities within the regional THEIA center (ART) in Bordeaux-Aquitaine, and Head of the ISPA remote sensing team. He coordinated the development of the L-MEB model for soil and vegetation in the Level-2 inversion algorithm of the ESA-SMOS Mission. His research interests are in microwave remote sensing of soil and vegetation, with the aim of monitoring soil moisture & the vegetation water status and dynamics at global scale. He has more than 120 papers in international peer-reviewed Journals (H-factor = 39) and he has been associate editor of *Remote Sensing of Environment* since 2014.

Mehdi Sbartaï is an associate professor at the University of Bordeaux since 2007 and co-leader of axis 3 (NDC/uncertainty propagation) of the GCE department within the I2 M laboratory. He got his PhD of the University of Toulouse and the PhD of the University of Sherbrooke/Canada in 2005 on a subject dealing with the inversion of non-destructive RADAR measurements for the characterization of concretes. He participates in numerous national and European projects (SENSO, ACDC, Duratinet, Evadeos, *etc.*). He developed extensive skills in the field of the NDC (Non Destructive Control) of building materials (concretes and wood), especially in the statistical data analysis and the NDT techniques mix. He is Associated with the ENDE project financed *via* the RSNR program (2014–2018).

Yann Kerr (M '88, SM '01, F'13) received the engineering degree from Ecole Nationale Supérieure de l'Aéronautique et de l'Espace, the M.Sc. degree in electronics and electrical engineering from Glasgow University, Glasgow, Scotland, UK, and the Ph.D. degree in Astrophysique Géophysique et Techniques Spatiales, Université Paul Sabatier, Toulouse, France. From 1980 to 1985 he was employed by CNES. In 1985 he joined LERTS; for which he was director in 1993–1994. He spent 19 months at JPL, Pasadena in 1987–88. He has been working at CESBIO since 1995 (deputy director 1995–1999 and director 2007–2016). His fields of interest are in the theory and techniques for microwave and thermal infra-red remote sensing of the Earth, with emphasis on hydrology, water resources management and vegetation monitoring. He has been involved with many space missions. He was an EOS principal investigator (interdisciplinary investigations), and PI and precursor of the use of the SCAT over land. In 1989 he started to work on the interferometric concept applied to passive microwave earth observation and was subsequently the science lead on the MIRAS project for ESA with MMS and OMP. He was also a Co-investigator on IRIS, OSIRIS and HYDROS for NASA. He was science advisor for MIMR and Co I on AMSR. He is a member of the SMAP Science Team. In 1997 he first proposed the natural outcome of the previous MIRAS work with what was to become the SMOS Mission to CNES, proposal which was selected by ESA in 1999 with him as the SMOS mission Lead-Investigator and Chair of the Science Advisory Group. He is also in charge of the SMOS science activities coordination in France. He has organised all the SMOS workshops, and was guest editor on three IEEE Special issues and one RSE. He is currently involved in the exploitation of SMOS data, in the Cal Val activities and related level 2 soil moisture and level 3 and 4 development and SMOS Aquarius SMAP synergistic uses and on the soil moisture essential climate variable. He is also working on the SMOS-Next concept and is involved in both the Aquarius and SMAP missions. He received the GRSS certificate of recognition for leadership in development of the first synthetic aperture microwave radiometer in space and success of the SMOS mission, and the ESA team award. He was nominated Highly cited scientist by Thomson Reuters in 2015.